Composition-induced metal-semiconductor-metal crossover in half-Heusler $Fe_{1-x}Ni_xTiSb$

J. Toboła,* L. Jodin, P. Pecheur, and H. Scherrer
Laboratoire de Physique des Matériaux, Ecole des Mines, Parc du Saurupt, 54042 Nancy Cedex, France

G. Venturini and B. Malaman
Laboratoire de Chimie du Solide Mineral, Université Henri Poincaré, Vandoeuvre-les-Nancy, 54042 Nancy Cedex, France

S. Kaprzyk
Faculty of Physics and Nuclear Techniques, University of Mining and Metallurgy, Al. Mickiewicza 30, 30-059 Krakow, Poland
(Received 9 April 2001; published 19 September 2001)

Structural and electrical transport properties of half-Heusler $Fe_{1-x}Ni_xTiSb$ solid solutions have been investigated using x-ray diffraction, ^{57}Fe Mössbauer spectroscopy, resistivity, and thermopower measurements. The electronic structure of the compounds was studied using the Korringa-Kohn-Rostoker coherent potential approximation (KKR-CPA). The resistivity curves measured over the 80–800 K temperature range show a remarkable modification of $\rho(T)$ versus x in $Fe_{1-x}Ni_xTiSb$, i.e., a metallicke character both in Fe-rich ($x=0.25$) and Ni-rich ($x=0.75$) samples and a semiconductinglike behavior near $x=0.5$. Moreover, the room-temperature Seebeck coefficient S changes from highly positive in $Fe_{0.6}Ni_{0.4}TiSb$ to highly negative in $Fe_{0.4}Ni_{0.6}TiSb$, while S is near zero in the $x=0.25$ and $x=0.75$ compositions. Based on the KKR-CPA results, the electrical transport properties of $Fe_{1-x}Ni_xTiSb$ arise from the appearance of an energy gap at the Fermi level for the $x=0.5$ content. This electronic structure feature indicates that FeTiSb and NiTiSb can be seen as one-hole and one-electron compounds, respectively, explaining a change in sign of the Seebeck coefficient in disordered phases near $x=0.5$.

DOI: 10.1103/PhysRevB.64.155103 PACS number(s): 61.10.−i, 61.18.Fs, 71.20.−b, 71.23.−k

I. INTRODUCTION

$Fe_{1-x}Ni_xTiSb$ crystallizes in the fcc structure over the whole concentration range and belongs to the well-known group of the half-Heusler systems. These compounds usually involve two different transition metals (also rare earth or noble elements) and one sp element such as Sn, Sb, or Bi. The crystal structure of the half-Heusler phase (F-43m) can be derived from the normal Heusler phase ($Fm3m$), consisting of four interpenetrating fcc sublattices, displaced along the body diagonal of the unit cell: (0,0,0), (1/4,1/4,1/4), (1/2,1/2,1/2), and (3/4,3/4,3/4), if one of the equivalent sublattices is vacant (Fig. 1). The crystal structure of Fe(Ni)TiSb can also be viewed as the rocksalt-type TiSb structure, where half of the tetrahedral sites are filled by heavier transition-metal atoms in an ordered way. Semiconductors, semimetals, normal Pauli metals, weak ferromagnets, and antiferromagnets as well as strong half-metallic ferromagnets exist in the half-Heusler series. Recent studies on the magnetic and transport properties of these phases have shown intriguing thermoelectrical behaviors,[1–5] giant magnetoresistance,[6] and localization effects.[7,8] Moreover, the variety of physical behaviors observed in the half-Heusler series seems to be related to strong modifications of the electronic structure near the Fermi level when changing the number of valence electrons [valence electron count (VEC)].[9,10]

The ordered compounds NiMSn (M=Ti, Zr, Hf),[2,3,11,12] CoMSb (M=Ti, Zr, Hf),[13–15] and FeMSb (M=V, Nb) (Refs. 5 and 21) display semiconducting or semimetallic character of resistivity. Electronic structure calculations with the use of various band theory methods[5,9,16–22] collectively conclude that in the aforementioned VEC=18 half-Heusler compounds there is a gap (E_g) at nine completed bands. The computed value of E_g strongly depends on the system investigated and varies from 0.29 eV (NiYSb) to 0.95 eV (CoTiSb) as demonstrated, for example, from the Korringa-Kohn-Rostoker (KKR) method.[9,10]

Note, however, that the energy gap deduced from fitting the resistivity curves to an activation law was found to be significantly smaller than the theoretical results. In NiMSn

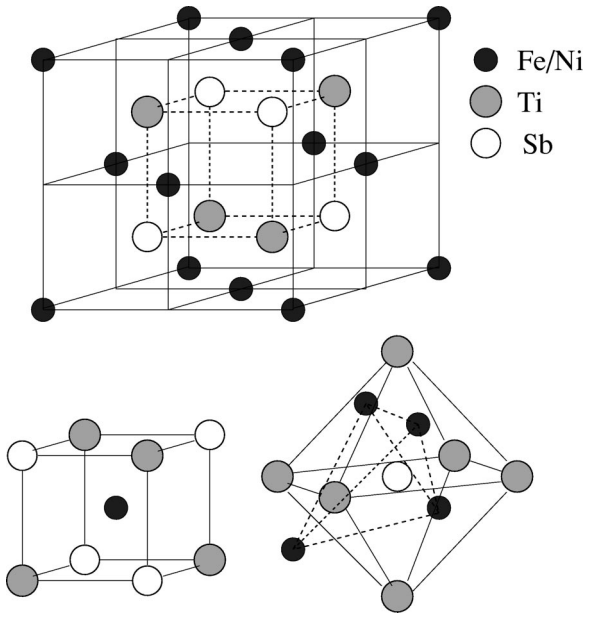

FIG. 1. The crystal structure and atomic coordinations in half-Heusler (Fe-Ni)TiSb.

(M=Ti, Zr, Hf), for example, E_g was estimated near 0.1–0.2 eV,[12] whereas the respective computed values are in the 0.4–0.5 eV range.[16,18] Atomic disorder often observed in the half-Heusler samples may substantially modify the transport properties. Indeed, a tendency of shrinking and then vanishing of the energy gap at the Fermi level was illustrated theoretically both in semiconducting[16,23] and half-metallic phases.[24] While the VEC=18 half-Heusler systems exhibit energy gap behavior, compounds richer or poorer in electrons are metals with either ferromagnetic or paramagnetic properties. This was evidenced in many experiments (see, for instance, Ref. 25).

It was believed from the rather common peculiarities of the electronic structure of the half-Heusler phases[10] that the energy gap at the Fermi edge might also appear in the solid solutions, when coming close to the critical value of the VEC. This prompted us to select $Fe_{1-x}Ni_xTiSb$ for electronic structure and transport property investigations. As our system corresponds to the variation of the valence electron number from 17 (FeTiSb) to 19 (NiTiSb), the VEC=18 limit is reached at the 50-50 Fe-Ni concentration in $Fe_{1-x}Ni_xTiSb$. Recent studies[7,21] of parent compounds of the title alloy concluded that FeTiSb is a Curie-Weiss paramagnet with $\mu_{eff}=0.87\ \mu_B$, while NiTiSb is a Pauli paramagnet. Thus, both samples displayed metallic properties.

Stimulating aspects of the present work are of both experimental and theoretical nature. First, relying on resistivity and thermopower measurements we intend to detect ''opposite'' crossovers upon changing the alloy composition in $Fe_{1-x}Ni_xTiSb$. Initially (for $x \leqslant 0.5$), we expect a crossover from metalliclike to semiconductorlike behavior and for higher x contents a return to metallic properties. Roughly speaking, we expect to observe the appearance of semiconducting properties in a disordered phase alloyed from the FeTiSb and NiTiSb metals. Furthermore, such an electronic structure study of such a ''marginal'' material allows us to make a highly accurate test of the computational approach.

Noteworthy, unusual transport properties of $Fe_{1-x}Ni_xTiSb$ were suggested from the preliminary coherent potential approximation KKR-(CPA) calculations.

II. EXPERIMENTAL RESULTS

A. Sample preparation and structural analysis

The studied compounds have been prepared from stoichiometric amounts of homemade FeTiSb and NiTiSb ternary phases previously prepared from the elements. The corresponding mixtures were first melted in an induction furnace in a water-cooled copper crucible. The resulting ingots were sealed in silica tubes under argon and annealed for 1 week at 1073 K. FeTiSb and NiTiSb, being of less interest for our study, were annealed only 1 day. The purity of the sample was checked by powder x-ray diffraction (Guinier camera and CPS detector, Co Kα). An illustrative diffraction pattern of $Fe_{0.5}Ni_{0.5}TiSb$ is given in Fig. 2. The cell parameters were refined by a least-squares procedure from powder x-ray diffraction data recorded with high-purity silicon ($a=5.43082$ Å) as internal standard. The lattice constant in the $Fe_{1-x}Ni_xTiSb$ alloy (Table I) follows more or less a linear decrease versus the Ni content, thus in close agreement with Vegard's law. The refined lattice constants of the FeTiSb and NiTiSb compounds are close to the previously reported values.[26]

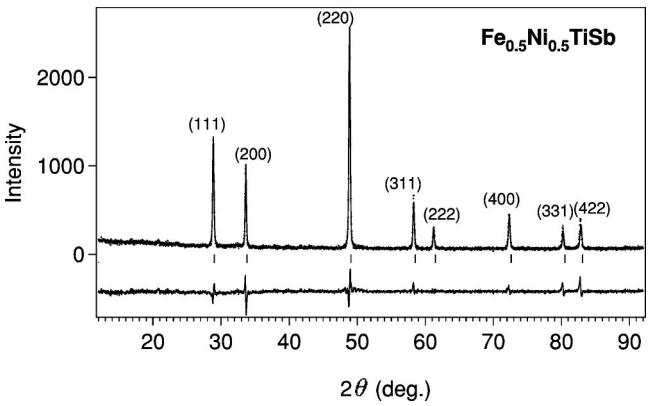

FIG. 2. X-ray diffraction pattern in $Fe_{0.5}Ni_{0.5}TiSb$.

To gain deeper insight into the atomic distribution in $Fe_{1-x}Ni_xTiSb$, x-ray diffraction and ^{57}Fe Mossbauer spectroscopy measurements have been used to study a possible disorder in the half-Heusler alloy $Fe_{0.5}Ni_{0.5}TiSb$.

An iron spectrum was collected at room temperature (RT) using a standard constant-acceleration spectrometer with a 10-mCi source of ^{57}Co in a rhodium matrix. The spectrum was fitted with a program,[27] which optimizes the quadrupole splitting EQ and the isomer shift δ with respect to α-Fe at room temperature for every doublet.

Two types of atomic disorder may occur in the half-Heusler structure for Fe/Ni atoms (due to a very close diffusion factor, iron and nickel atoms cannot be distinguished by x-ray diffraction): an antisite disorder on Ti or Sb positions and a partial occupation of a tetrahedral vacant site (as seen in Fig. 1). These possible atomic distributions could be checked through the value of the intensity ratios (I_{111}/I_{220} and I_{200}/I_{220}), which are correlated to the above-mentioned disorder. In Table II we give a comparison of the calculated intensity ratios for a perfectly ordered sample and different types of disorder (as large as 10%) with observed values. Surprisingly, it indicates that within the accuracy of the x-ray diffraction a weak antisite disorder (Fe/Ni-Sb) occurs in the present sample.

TABLE I. Room-temperature values of structural and transport parameters in $Fe_{1-x}Ni_xTiSb$.

x	a(Å)	$\rho(\mu\Omega\ \mathrm{m})$	$S(\mu V\,K^{-1})$
0.0	5.951(3)	–	–
0.25	5.924(3)	4.1	≈0
0.40	5.917(4)	19.1	124
0.50	5.910(3)	134.7	33
0.60	5.906(4)	90.8	−112
0.75	5.907(5)	4.2	≈0
1.00	5.884(2)	–	–

TABLE II. Observed and calculated intensity ratios in $Fe_{0.5}Ni_{0.5}TiSb$. Calculated intensities correspond to disorder of 10% between Fe/Ni and Ti (antisite Ti), Sb (antisite Sb), and vacancy (vac. site), respectively.

Type	I_{111}/I_{220}	I_{200}/I_{220}
Ordered	0.43	0.34
Antisite Ti	0.43	0.35
Antisite Sb	0.43	0.27
Vac. site	0.37	0.34
Experimental	0.41	0.28

The Mössbauer spectrum (Fig. 3) shows one strong line and a very weak line on the positive velocity side (Table III). The strongest doublet is attributed to the iron nucleus of the tetrahedral site. Nevertheless, Mössbauer spectroscopy would not allow distinguishing between the (0,0,0) and (1/2,1/2,1/2) tetrahedral sites due to their identical environments. As previously shown from x-ray diffraction data, a slight iron occupation of the Sb site occurs that corresponds well to the weak absorption line. The Mössbauer mean value of the iron occupation in this site is $\approx 6\%$, thus in full agreement with the structural investigations.

In conclusion we can say that the $Fe_{0.5}Ni_{0.5}TiSb$ sample presents a high degree of order ($>95\%$). Similar results have been obtained for other compositions with an antisite disorder smaller than 7%.

B. Transport measurements

1. Resistivity

The electrical resistivity curves $\rho(T)$ have been measured using the van der Pauw method. Samples were prepared as square pieces of approximately 4×4 mm^2 in surface and a thickness smaller than 1 mm, by cutting with a diamond wire. At low temperatures, silver epoxy paint was used to attach contacts to samples, while at high temperatures we applied molybdenum rod contacts. The measurement system allowed us to perform experiments within two temperature regimes, either at low (between 80 K and 350 K) or at high temperatures (between 350 K and 800 K).

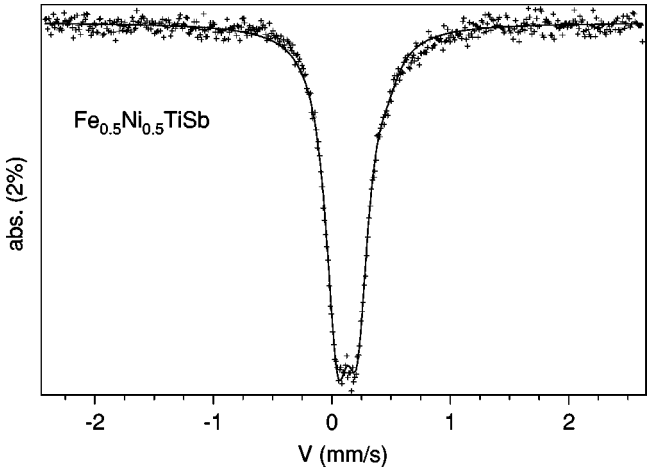

FIG. 3. Mossbauer spectrum in $Fe_{0.5}Ni_{0.5}TiSb$.

TABLE III. Room-temperature hyperfine parameters in $Fe_{0.5}Ni_{0.5}TiSb$. Γ, δ, and EQ are the Lorentz profile width, the isomer shift, and the quadrupole splitting, respectively. P is the relative area of the corresponding doublet, while χ^2 is the reduced χ square. Experimental error of Γ, δ, and EQ is ≈ 0.01 mm/s.

P	Site	Γ(mm/s)	δ(mm/s)	EQ(mm/s)	χ^2
94%	Tetrahedral	0.24	0.13	0.17	0.98
6%	Octahedral	0.24	0.19	0.47	0.98

Figure 4 shows the resistivity $\rho(T)$ curves in the 350–800 K temperature range for different compositions of the $Fe_{1-x}Ni_xTiSb$ alloy. At first sight, we conclude that the character of $\rho(T)$ apparently changes with increasing x concentration. We start our analysis from the boundary compositions. At $x=0.25$ and $x=0.75$, the resistivity increases with temperature in a metallic way. The $\rho(T)$ value measured at room temperature is of the order of a few $\mu\Omega$ m which is much higher than that of a good metal. Conversely, at $x=0.5$ the resistivity decreases with temperature in a semiconducting way. Simultaneously, ρ increases by a factor of about 30 with respect to the aforementioned metallic phases. For the $x=0.4$ and $x=0.6$ concentrations we obtain intermediate results. $Fe_{0.6}Ni_{0.4}TiSb$ has a resistivity which increases with temperature, tending to a constant value. $Fe_{0.4}Ni_{0.6}TiSb$ exhibits first a semiconducting behavior; then with increasing temperature ρ also tends to a constant value. If we distinguish metalliclike from semiconductinglike behavior using the change of sign of $d\rho/dT$, $Fe_{0.4}Ni_{0.6}TiSb$ is close to this limit. On the whole, the $\rho(T)$ results suggest a metal-semiconductor-metal crossover in $Fe_{1-x}Ni_xTiSb$ when x increases.

Similar changes in the resistivity characteristics in $Fe_{1-x}Ni_xTiSb$ can be found from low-temperature data.

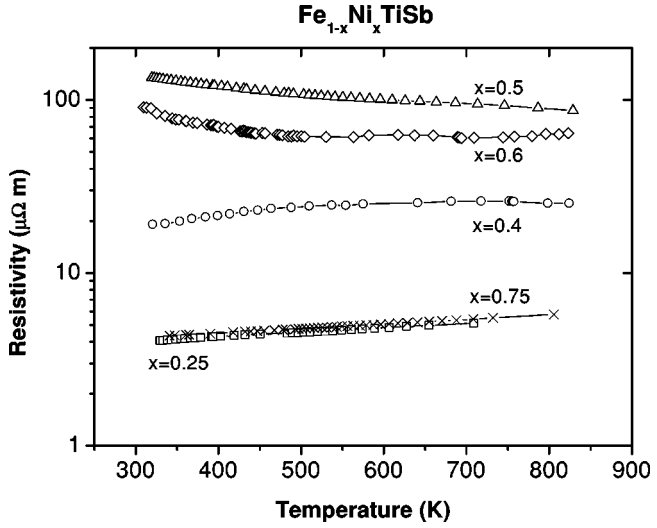

FIG. 4. High-temperature dependence of resistivity in $Fe_{1-x}Ni_xTiSb$.

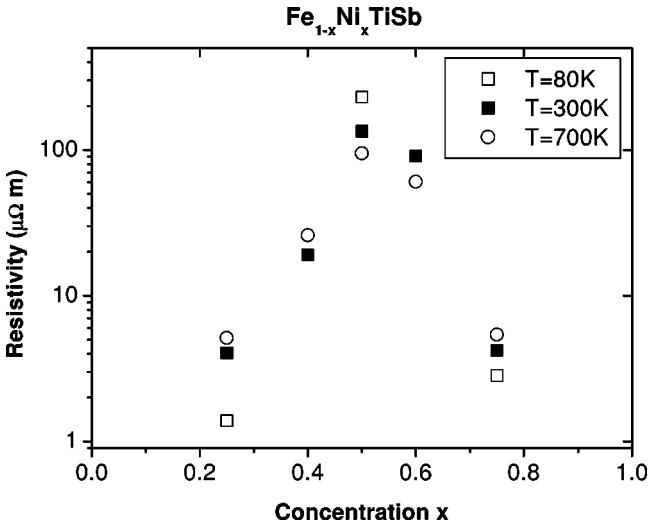

FIG. 5. Resistivity at 80, 300, and 700 K in $Fe_{1-x}Ni_xTiSb$.

Finally, Fig. 5 gathers the resistivity values measured at three selected temperatures ($T=80$, 300, and 700 K) in all investigated samples. This enables us to summarize the two aforementioned effects detected on the $Fe_{1-x}Ni_xTiSb$ resistivity curves: (1) a marked enhancement of the $\rho(T)$ value in the vicinity of $x=0.5$, unlike the $x=0.25$ and $x=0.75$ samples; (2) different temperature dependences of resistivity; metalliclike in Fe-rich and Ni-rich samples whereas semiconductinglike or semimetalliclike in the intermediate samples.

2. Thermopower

The thermopower was measured using the standard differential technique. In Fig. 6 we plot the evolution of the Seebeck coefficient S obtained at $T=300$ K versus the content x. In the Fe-rich compositions ($x=0.25$), S was found to have a small value, which is characteristic of metals. Such a result corresponds well to the above-mentioned resistivity data, also exhibiting metalliclike behavior. For $x=0.4$ a large and positive value of S was observed, indicating heavily doped p-type material, the conductivity attributed to holes. This is also in line with the semimetallic character of resistivity measured in this sample. In the $Fe_{0.5}Ni_{0.5}TiSb$ semiconductor, S is markedly smaller than in the former sample but also has a positive value. This indicates that holes still dominate over electrons. The tendency of S to decrease with increasing x continues, turning the Seebeck coefficient in to a large and negative value in the $Fe_{0.4}Ni_{0.6}TiSb$. This gives evidence of a change in carrier type, where electrons visibly play a dominant role in conduction. The result obtained in the $x=0.6$ sample can be contrasted to the $x=0.4$ case, in which S is positive but of a comparable absolute value (Table I). For higher concentrations ($x=0.75$) the Seebeck coefficient again acquires a negligible value.

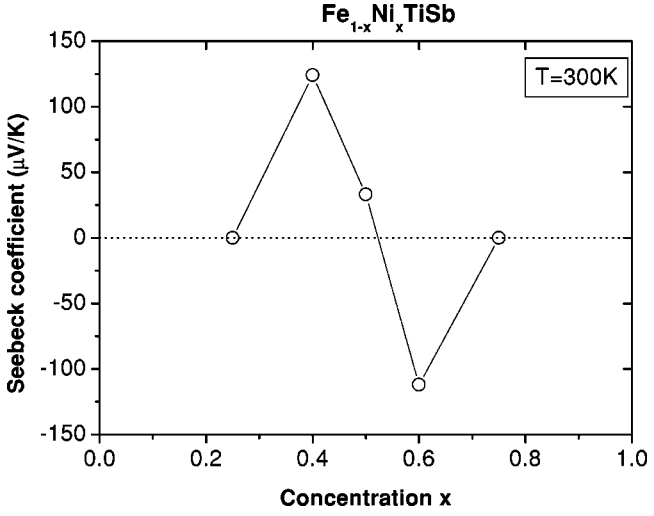

FIG. 6. Seebeck coefficient at $T=300$ K in $Fe_{1-x}Ni_xTiSb$. A line connecting experimental points is added as a guide to the eye.

The large values of S observed near the metal-semiconductor crossover, in $Fe_{0.6}Ni_{0.4}TiSb$ and $Fe_{0.4}Ni_{0.6}TiSb$, are also expected from some models,[28] predicting near-divergent behavior of S in a disorder-driven metal-insulator transition.

C. Electronic structure calculations

The electronic structure computations on the disordered $Fe_{1-x}Ni_xTiSb$ (with $x=0.0$, 0.25, 0.4, 0.5, 0.6, 0.75, and 1.0) were performed by the charge-self-consistent Korringa-Kohn-Rostoker method with the coherent potential approximation. The crystal potential of muffin-tin form was constructed within the local density approximation (LDA) approximation, using the von Barth–Hedin[29] formula for the exchange-correlation part. The Fermi energy was determined precisely (≈ 0.1 mRy) via the generalized Lloyd formula,[30] using an elliptic contour in the complex energy plane. The KKR-CPA Green function was computed on a 75 special **k**-point mesh in the irreducible part of the Brillouin zone. The self-consistency cycles were repeated until input-output differences of potentials and charges inside muffin-tin spheres were of order 1 mRy and $10^{-3}e$, respectively. All calculations employed a maximum angular momentum $l_{max}=2$. For the final potentials, the total density of states (DOS), site-decomposed DOS, and l-decomposed partial DOS were computed using the tetrahedral **k**-space integration technique. More details concerning the KKR-CPA methodology used in our computations can be found in Ref. 31.

In the cubic phase Fe (Ni), Ti and Sb atoms occupied (0,0,0) (3/4,3/4,3/4) and (1/4,1/4,1/4) sites, respectively (note that a different origin can also be used). An empty sphere was added on the (1/2,1/2,1/2) position, increasing the packing ratio to 68%. The experimental values of the lattice constant a, as listed in Table I, were applied to our calculations with the use of equivalent values of muffin-tin radii for basis atoms ($r_{MT}=\sqrt{3}/8a$).

D. FeTiSb and NiTiSb

The electronic structure of FeTiSb and NiTiSb was partly discussed in previous works,[7,10] so that we only briefly recall the main KKR results. In Fig. 7, the nonpolarized total and site-decomposed DOS in FeTiSb and NiTiSb are shown. An

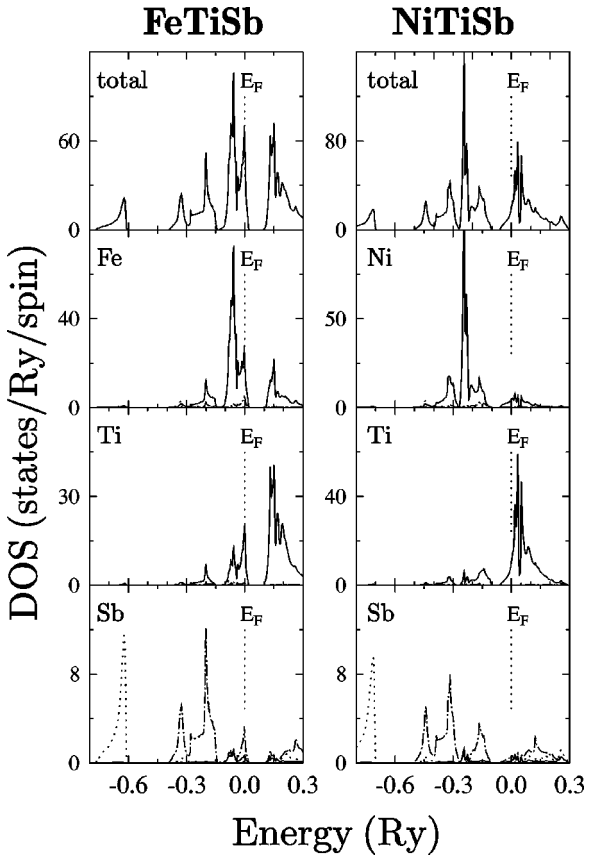

FIG. 7. Nonpolarized KKR total and *l*-decomposed DOS on inequivalent atoms in FeTiSb and NiTiSb (E_F is at zero). The *s*, *p*, and *d* contributions are plotted by dotted, dashed, and solid lines, respectively.

apparent feature on the spectra of both compounds is the existence of an energy gap in the density of states at nine completed bands [easily observed on dispersion curves $E(\mathbf{k})$, Fig. 8]. This seems to be a rather general behavior of the electronic structure of half-Heusler compounds.[10] The energy gap arises essentially from the hybridisation of *d* states coming from different transition-metal atoms with *p* states on Sb, splitting the electronic spectra of FeTiSb and NiTiSb into two energy regions. The DOS above the gap is dominated by *d* states on Ti, overlapping with *d*-state Fe (Ni) to various extents. Electronic states lying just below this gap are dominated by *d* state on Fe (Ni), being hybridized basically with *d* states on Ti and *p* states on Sb. The lowest-lying electronic states apart from the valence band correspond mostly to *s* states on Sb.

Despite the above-mentioned similarity of electronic structure observed in both compounds (an intraband gap) the DOS shapes of FeTiSb and NiTiSb are rather different. However, a much more obvious distinction between the electronic structures of the compounds is related to the Fermi level position with respect to the energy gap. This should have a considerable effect on the transport properties. In FeTiSb, E_F is located below the gap in the vicinity of the large and sharp DOS peak attributed mostly to *d* states on Fe. On the other hand, in NiTiSb (accommodating more electrons) E_F lies above the gap in a smoothly increasing DOS and thus partly filling a conduction band.

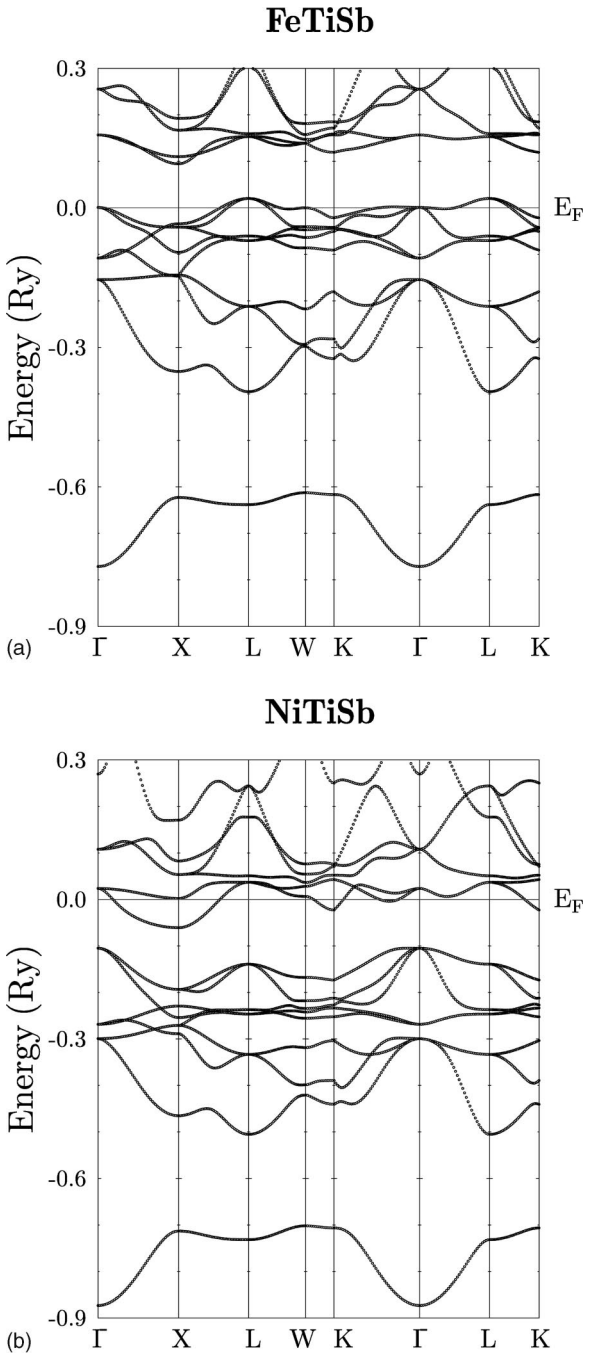

FIG. 8. High-symmetry dispersion curves $E(\mathbf{k})$ in FeTiSb (top) and NiTiSb (bottom). E_F is at zero.

The presence of the energy gap at the nine bands allows us to consider FeTiSb and NiTiSb compounds as either one-hole or one-electron systems, respectively.

In the purely ordered half-Heusler structure of FeTiSb (with $a=5.951$ Å) the spin-polarized KKR computation results in a ferromagnetic state with a magnetic moment of $0.8\mu_B$ (per f.u.) due to local magnetic moments on Fe ($0.6\mu_B$) and Ti ($0.1\mu_B$). Note that the Fermi level was found in the vicinity of strongly varying DOS or even the gap. Thus, FeTiSb is close to the magnetic instability which may explain a disagreement between the theoretical and experi-

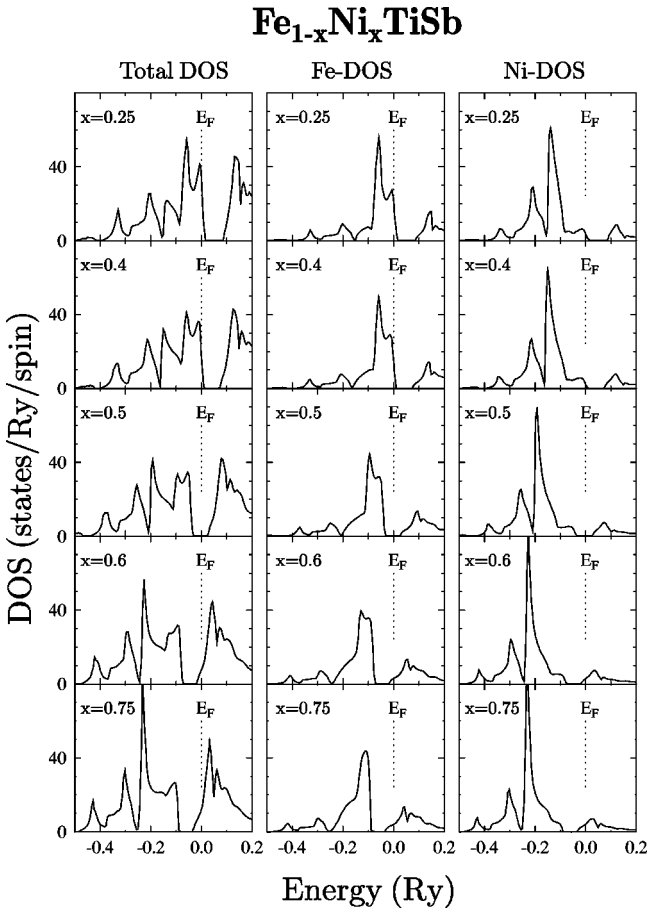

FIG. 9. KKR-CPA total, Fe-site, and Ni-site DOS in $Fe_{1-x}Ni_xTiSb$ (E_F is at zero).

mental results. In spite of the Curie-Weiss behavior of FeTiSb, no magnetic ordering was observed down to $T=1.5$ K.[21] Conversely, the KKR-CPA on a disordered $(Fe_{0.5}E_{0.5})_2TiSb$ (E denotes vacant site), in which Fe atoms are distributed randomly on two equivalent sites in the $Fm3m$ structure, gives a nonmagnetic ground state, in agreement with the experimental data. However, in this disordered case the energy gap is no longer seen.

From the KKR calculations the ground state of NiTiSb was found to be nonmagnetic with a low DOS at the Fermi level attributed mostly to *d* states on Ti. This result supports Pauli paramagnetic properties observed experimentally.[7]

E. $Fe_{1-x}Ni_xTiSb$ solid solutions

The KKR-CPA electronic structure of $Fe_{1-x}Ni_xTiSb$ is presented in Fig. 9. We show the total as well as the Fe and Ni site-decomposed DOS in five compositions, which correspond to the experimental samples. At a first glance, we see that the total DOS shape (left column in Fig. 10) markedly changes upon varying the alloy composition. It results from strong DOS modifications seen on Fe and Ni atoms (middle and right columns in Fig. 9). Remarkably, the intraband gap detected in the DOS in FeTiSb (above E_F) and NiTiSb (below E_F) is observed over the whole range of concentration of $Fe_{1-x}Ni_xTiSb$. This gap gradually shrinks with the Ni increase from about 1 eV (FeTiSb) to 0.6 eV (NiTiSb).

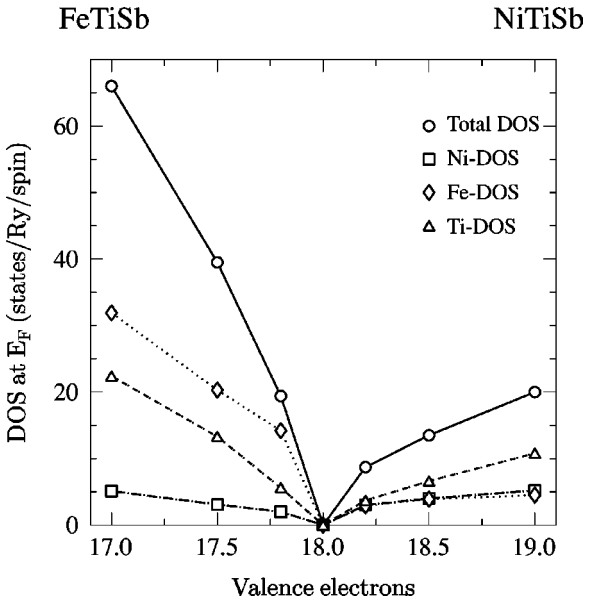

FIG. 10. KKR-CPA DOS at E_F in $Fe_{1-x}Ni_xTiSb$.

Looking at the position of the Fermi level at various contents we note that it falls precisely into the gap at $x=0.5$ which corresponds to a semiconducting state (Fig. 10). Indeed, such a behavior was evidenced in the $Fe_{0.5}Ni_{0.5}TiSb$ sample from the resistivity measurements showing a decrease of $\rho(T)$ vs T. On the other hand, in Fe-rich ($x=0.25$) and Ni-rich ($x=0.75$) samples, the DOS at E_F is finite which agrees well with the metalliclike character of $\rho(T)$ observed experimentally. The $x=0.4$ and $x=0.6$ systems are found to be intermediate cases with relatively low but finite DOS at E_F. In resistivity experiments they exhibit semiconductinglike or semimetallic behaviors.

Noteworthy, in the Fe-rich samples the DOS at E_F varies in apparently different ways than in Ni-rich samples. By calculating the energy derivative of the DOS in the vicinity of E_F, we may conclude that $dn(E)/dE$ is significantly larger in $Fe_{0.6}Ni_{0.4}TiSb$ than in $Fe_{0.4}Ni_{0.6}TiSb$. Furthermore, $dn(E)/dE$ should change sign when the Fermi level crosses the gap at $x=0.5$. A change in sign of the Seebeck coefficient S between $Fe_{0.6}Ni_{0.4}TiSb$ (p type) and $Fe_{0.4}Ni_{0.6}TiSb$ (n type) is expected from DOS characteristics.

In the semiconducting $Fe_{0.5}Ni_{0.5}TiSb$ the DOS shape at the top of the valence states (attributed to holes) and at the bottom of the conduction states (attributed to electrons) is not similar. As in random systems we cannot properly derive the effective masses of the carriers from the $1/m^*=\partial^2E/\partial k^2$ formula; we may, however, approximately relate hole and electron masses to the DOS variation (dn/dE) on both sides of the gap. In the $x=0.5$ case an average hole m^* is significantly larger than that of electrons, which may correspond to the positive value of the Seebeck coefficient experimentally detected in this sample.

III. CONCLUSIONS

$Fe_{1-x}Ni_xTiSb$ (with $x=0.25$, 0.4, 0.5, 0.6, 0.75) solid solutions were synthesized in the half-Heusler structure. X-ray

diffraction and ^{57}Fe Mössbauer spectroscopy measurements reveal that the aforementioned samples are pure and iron atoms are distributed randomly with Ni atoms mainly on one crystallographic site ($>95\%$). A small disorder ($\approx 5\%$) occurs rather between Fe/Ni and Sb sites than Ti sites.

The resistivity curves measured in the 80–800 K temperature range show a remarkable modification of $\rho(T)$ upon increasing x in $Fe_{1-x}Ni_xTiSb$, i.e., a metalliclike character of $\rho(T)$ both in the $x=0.25$ and $x=0.75$ samples, while a semiconductinglike behavior in the vicinity of $x=0.5$. This phenomenon can be directly related to the appearance of a real energy gap in the density of states at E_F as precisely detected from the KKR-CPA computations. A finite DOS is computed in samples experimentally found as metalliclike.

From the thermopower measured at 300 K, we observe that the Seebeck coefficient S changes sign when approaching the $x=0.5$ concentration from highly positive in $Fe_{0.6}Ni_{0.4}TiSb$ to highly negative in $Fe_{0.4}Ni_{0.6}TiSb$. The thermopower of Fe-rich and Ni-rich compositions is close to zero.

This can also be interpreted through the presence of the energy gap as well as the specific variation of the KKR-CPA density of states near the top of the valence band and the bottom of the conduction band, respectively.

It seems interesting to compare the electronic structure and the transport properties of $Fe_{1-x}Ni_xTiSb$ near $x=0.5$ to those of the CoTiSb compound. From the resistivity measurements this 18-valence-electron compound exhibits semiconducting properties.[13] Furthermore, the resistivity character and the Seebeck coefficient of CoTiSb drastically change upon doping.[15] This compound was found to be a wide gap semiconductor ($E_g=0.95$ eV) from band structure calculations.[9]

Such physical properties of CoTiSb are closely related to the phenomena observed in $Fe_{1-x}Ni_xTiSb$ with x near 0.5.

ACKNOWLEDGMENT

We are indebted to Dr. E. McRae (LCSM UHP, Vandoeuvre-les-Nancy) for his critical reading of the manuscript.

*Also at Faculty of Physics and Nuclear Techniques, University of Mining and Metallurgy, Al. Mickiewicza 30, 30-059 Krakow, Poland. Electronic address: tobola@ftj.agh.edu.pl

[1] S.J. Poon, Semicond. Semimetals **70**, 37 (2001), and references therein.
[2] H. Hohl, A.P. Ramirez, C. Goldman, G. Ernst, B. Wolfing, and E. Bucher, J. Phys.: Condens. Matter **11**, 1697 (1999).
[3] C. Uher, J. Young, J. Hu, D.T. Morelli, and G.P. Meisner, Phys. Rev. B **59**, 8615 (1999).
[4] K. Mastonardi, D. Young, C.C. Wang, P. Khalifah, and R.J. Cava, Appl. Phys. Lett. **74**, 1415 (1999).
[5] D. Young, P. Khalifah, R.J. Cava, and A.P. Ramirez, J. Appl. Phys. **87**, 317 (2000).
[6] J. Pierre and I. Karla, J. Magn. Magn. Mater. **217**, 74 (2000).
[7] K. Kaczmarska, J. Pierre, J. Tobola, and R.V. Skolozdra, Phys. Rev. B **60**, 373 (1999).
[8] J. Pierre, K. Kaczmarska, and J. Tobola, Eur. Phys. J. B **18**, 247 (2000).
[9] J. Tobola, S. Kaprzyk, R.V. Skolozdra, and M.A. Kouacou, J. Phys.: Condens. Matter **10**, 1013 (1998).
[10] J. Tobola and J. Pierre, J. Alloys Compd. **296**, 243 (2000).
[11] F.G. Aliev, F.G. Brandt, V.V. Moshchalkov, V. Kozyrkov, R.V. Skolozdra, and A.I. Belogorov, Z. Phys. B **75**, 167 (1989).
[12] F.G. Aliev, V.V. Kozyrkov, V. Moshchalkov, R.V. Skolozdra, and K. Durczewski, Z. Phys. B **80**, 353 (1990).
[13] M.A. Kouacou, J. Pierre, and R.V. Skolozdra, J. Phys.: Condens. Matter **7**, 7373 (1995).
[14] Y. Xia, S. Bhattacharya, V. Ponnambalam, A.L. Pope, S.J. Poon, and T.M. Tritt, J. Appl. Phys. **88**, 1952 (2000).
[15] Y. Xia, V. Ponnambalam, S. Bhattacharya, A.L. Pope, S.J. Poon, and T.M. Tritt, J. Phys.: Condens. Matter **13**, 77 (2001).
[16] S. Ogut and K.M. Rabe, Phys. Rev. B **51**, 10443 (1995).
[17] H. van Leuken and R.A. de Groot, Phys. Rev. Lett. **74**, 1171 (1995).
[18] J. Tobola, S. Kaprzyk, R.V. Skolozdra, and M.A. Kouacou, J. Magn. Magn. Mater. **159**, 192 (1996).
[19] S. Ishida, T. Masaki, S. Fujii, and S. Asano, Physica B **42**, 363 (1997).
[20] A. Slebarski, A. Jezierski, A. Zygmunt, S. Mahl, and M. Neumann, Phys. Rev. B **57**, 9544 (1998).
[21] K. Kaczmarska, J. Pierre, J. Tobola, and R.V. Skolozdra, J. Magn. Magn. Mater. **187**, 210 (1998).
[22] P. Larson, S.D. Mahanti, S. Sportouch, and M.G. Kanatzidis, Phys. Rev. B **59**, 15660 (1999).
[23] J. Tobola, P. Pecheur, H. Scherrer, J. Pierre, and S. Kaprzyk, in *Proceedings of 19th International Conference on Thermoelectrics*, Cardiff 2000, edited by D. M. Rowe (Babrow Press, Wales UK, 2001), pp. 135–142.
[24] D. Orgassa, H. Fujiwara, T.C. Schulthess, and W.H. Butler, Phys. Rev. B **60**, 13237 (1999).
[25] J. Pierre, R.V. Skolozdra, J. Tobola, S. Kaprzyk, C. Hordequin, M.A. Kouacou, I. Karla, R. Currat, and E. Lelievre-Berna, J. Alloys Compd. **262-263**, 101 (1997).
[26] P. Villars and L. D. Calvert, in *Pearson's Handbook on Intermetallic Phases* (ASM International, Metals Park, Ohio, 1991).
[27] G. Le Caer (private communication).
[28] K. Durczewski and A. Krzywicki, Phys. Rev. B **58**, 10302 (1998).
[29] U. von Barth and L. Hedin, J. Phys. C **5**, 1629 (1972).
[30] S. Kaprzyk and A. Bansil, Phys. Rev. B **42**, 7358 (1990).
[31] A. Bansil, S. Kaprzyk, P.E. Mijnarends, and J. Tobola, Phys. Rev. B **60**, 13396 (1999).